Combining High-Resolution TEM on Graphene With In-Situ Hall Measurements

Benedikt Westenfelder

We describe an approach allowing high-resolution transmission electron microscopy (HRTEM) on specimens like graphene and the investigation on their electronic transport properties at the same time. The experimental set-up presented here is based on the modification of a commercial TEM specimen holder and on a specially designed sample carrier. A customized Hall sensor confirms that the local magnetic field provided by the microscope's objective lens is sufficiently high and homogenous for in-situ Hall effect measurements. Finally, we discuss first experimental results on defective graphene specimens. Indeed, our data reveals great potential in terms of correlating the information which we gain from HRTEM images with the corresponding transport properties, but also indicates further tasks and challenges.

1. Introduction

Not later then 2010, when the Nobel Prize went to Andre Geim and Konstantin Novoselov, the novel material graphene, basically a single atomic layer of hexagonally arranged carbon atoms, got well known for it's large number of outstanding properties [1]. Without further ado, it could be called the thinnest material on earth providing highest mechanical stability at the same time. Due to its very low thickness it is also extremely transparent (only 2.3 % broadband absorption) and interestingly, it is still an exceptionally good conductor [2,3]. For instance, it provides mobilities of $1.2 \cdot 10^5\,\mathrm{cm}^2/(\mathrm{Vs})$ near room temperature ($T = 240\,\mathrm{K}$) and relatively high sheet carrier densities of $2 \cdot 10^{11}\,\mathrm{cm}^{-2}$ [4]. Even if its surface its not functionalized, i.e., if its surface could be considered as chemically inert, its very large surface-area-to-volume ratio provides large potential for sensing applications [5, 6]. The excellent sensing functionality has been confirmed experimentally several times, however without detailed understanding in terms of the real interaction mechanisms behind. It shouldn't be only a matter of quantifying the actual number of adsorbed molecules: As known from theoretical studies, smallest changes on their detailed atomic position can be induced by different temperatures and affect the electronic interaction differently [7]. This ranges from small shifts of the Fermi level to significant modifications of the intrinsic electronic band structure, i.e., the formation of a band gap. The same holds when we consider defects instead of a perfect graphene lattice. The transport properties, i.e., the carrier mobility, might strongly depend on the number and the sort of defects. Here, we could distinguish roughly between grain boundaries originating inevitably from the growth process or even intentionally implanted point defects, e.g., in order to modify the transport properties [8]. The latter is the sort of defect which we

have chosen for illustrating our approach. In terms of a proof-of-principle approach, we demonstrate how imaging on an atomic scale with simultaneous transport measurements could be performed for revealing deeper insights into the world of defects and their role on the transport properties.

2. Experimental Requirements

The specimens were studied by aberration-corrected HRTEM (AC-HRTEM) performed by a TITAN (80-300) FEI microscope at only 80 kV to avoid knock-on damage [9]. In order to induce intentional defects the microscope has been switched to 300 kV in between and switched back to 80 kV for imaging. Changes on the electronic properties in terms of the sheet resistance have been investigated according to the Van der Pauw method (see ref. [10]) via in-situ four-point probe electrical measurements. Once the magnetic field of the microscope's objective lens had been determined, also the carrier concentration and the Hall mobility could be evaluated.

2.1 The microscope's 'internal' field

We fabricated a specially designed Hall sensor in order to determine the microscope's 'internal' magnetic field (induced by the objective lens) at 80 kV operation (Fig. 1a). The sensor itself consists of a $8 \times 8\,\mu m^2$ mesa structure based on a 1 µm thick n-doped GaAs top layer grown on semi-insulating GaAs (Fig. 1b). Its tiny dimensions have been chosen in order resolve possible magnetic field variations with correspondingly high spatial resolution. The mesa is located centrally to four electrical contact pads. After mounting the Hall sensor into an appropriate TEM specimen holder, the Van der Pauw method has been applied for ex-situ calibration and subsequently for in-situ scanning of the magnetic field at all possible specimen positions. The field was found to be considerably homogeneous corresponding to 1.224 T±0.001 T at 80 kV.

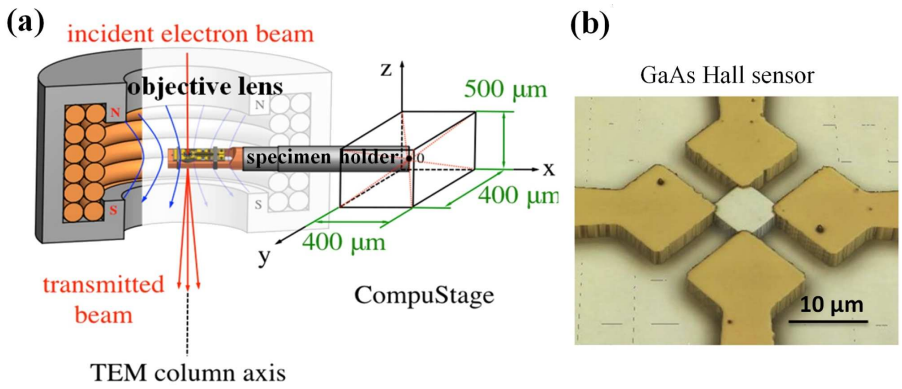

Fig. 1: (a) Scheme of the measurement concept. The magnetic field gets monitored for all possible specimen positions. (b) Three-dimensional (3D) confocal optical micrograph of the GaAs-based mesa structure and its four contact electrodes.

2.2 TEM specimen holder

Our single tilt heating holder from Gatan, Inc. (Model 628) provides six electrical feedthroughs for in-situ electrical experimentation accessible via six metallic pins located behind the actual specimen location (Fig. 2a). However, it still requires some modifications in order obtain feasible access to four wires at least — any wire-bonding-based solution would be too delicate. For this reason, we added a ceramic plate that includes four U-shaped metal sticks bridging the large distance between pins and specimen location (Fig. 2b). The small metal sticks are guided and stabilized by an insulating ceramic ring. The sticks also act as spring contacts when the Hall sensor gets mounted upside down and fixed by a hollow lock screw.

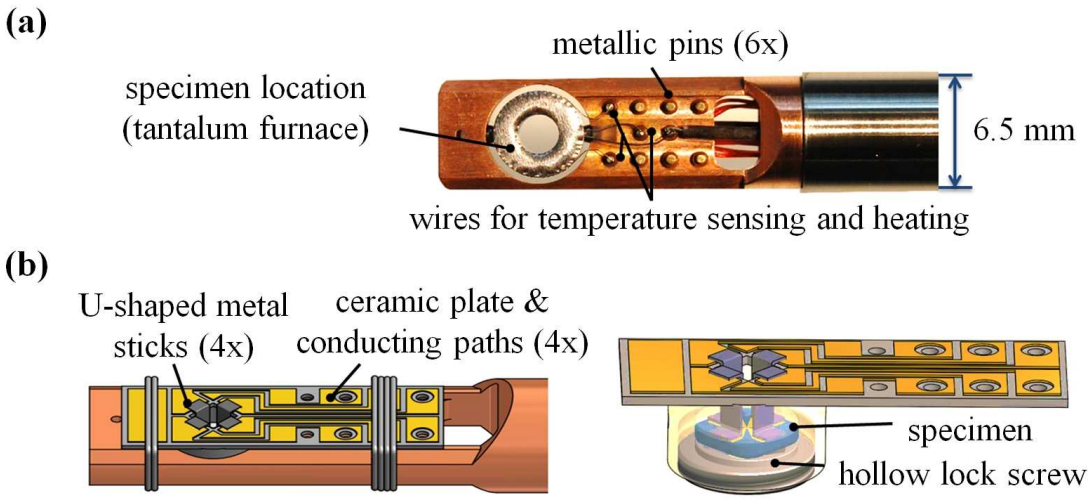

Fig. 2: (a) Photograph of the original front part of the specimen holder. (b) Front part after adding a ceramic plate with embedded conducting paths and four U-shaped metal sticks.

2.3 Graphene specimen

Just as for the Hall sensor, also the graphene specimens must provide large contact areas and fulfill standard TEM specimen size requirements. The specimens here are based on a silicon frame covered with an insulating SiN_x top layer of 750 nm (Fig. 3a). Furthermore, each specimen has a SiN_x window that includes a central opening. This is the area of interest for HRTEM imaging. On top of that opening, the graphene membrane is be suspended between four electrodes. The electrodes (200 nm) have been embedded into the SiN_x top layer in order to avoid topography-induced curvatures resulting in strain. The graphene samples (single layers and bilayers) are fabricated via mechanical exfoliation. After transferring the graphene on top of the electrodes [11], we applied optical lithography and reactive ion etching in order to obtain a fully freestanding graphene structure. The electrode pitch has been chosen as small as possible in order to avoid large fragileness and the necessity of critical point drying. The pitch corresponds to 1.5 µm — small enough, but close to the limit which can be achieved with optical lithography (Figs. 3b,c).

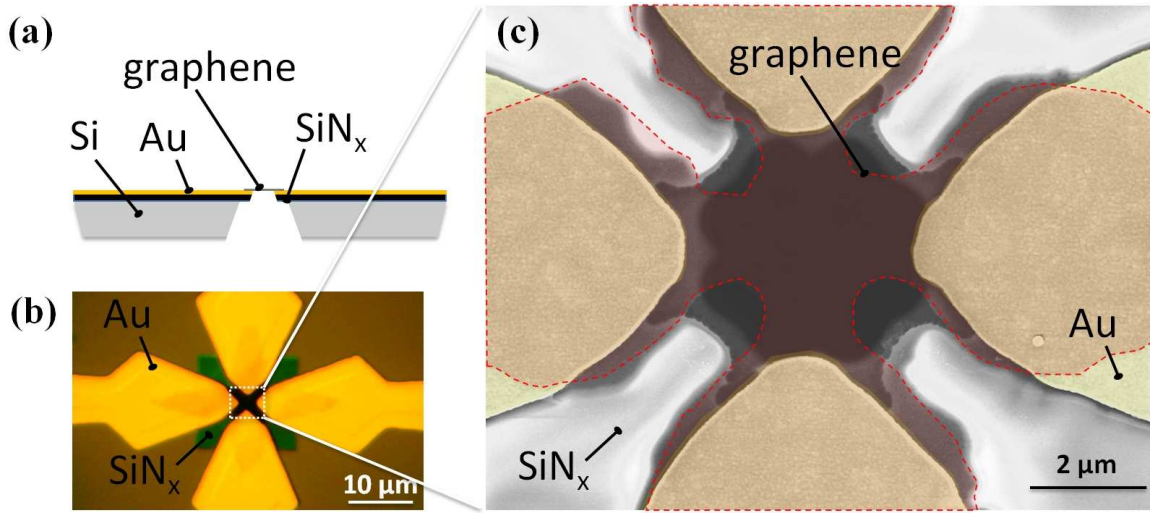

Fig. 3: (a) Schematic diagram of the graphene specimen. (b) Optical micrograph of the real specimen (central part). (c) SEM micrograph of the real specimen (central part) revealing the lithographically patterned graphene sheet.

3. Experiments

After the specimen preparation and a final cleaning procedure in various organic solutions, the graphene surface remains highly contaminated, not visibly but on the microscopic scale. This amount of residues typically changes electronic properties so drastically that the mobility is reduced by even two orders of magnitude. However, a clean initial condition is required in order to correlate structural changes like defects on the atomic scale with a change in the electronic transport properties.

In order to remove all residues, the sample (graphene bilayer) has been pre-annealed in the TEM column by applying a heating function integrated into the specimen holder. The sample has been baked gently at 200 °C for 1 hour resulting already in a significant increase of the mobility ($314\,\mathrm{cm^2/(Vs)}$ to $1708\,\mathrm{cm^2/(Vs)}$) and decrease of the carrier concentration ($3 \cdot 10^{-12}\,\mathrm{cm^{-2}}$ to $4 \cdot 10^{-12}\,\mathrm{cm^{-2}}$). So, the mobility has now been interpreted as an indicator for the sample's cleanness. We might expect a rather clean sample now, but first images revealed still a large degree of contamination. Apparently the annealing temperature was not high enough.

It has been found, once a contaminated sample has been irradiated, i.e., imaged, the residues cannot be driven off anymore. For this reason, we had to use new samples for another pre-annealing at *higher* temperatures. This time, not the entire specimen, but only the freestanding graphene membrane gets heated via Joule heating. This happened via driving a current through the graphene flake. The current annealing procedure has the advantage of achieving temperatures until the regime of 2000 K [12]. There is only one difficulty: we do not have a direct measure for the local temperature, but just a rough idea by the electrical power that is consumed by the membrane. Furthermore, it is not possible to watch/irradiate the sample during the annealing procedure. So there is a large risk of damaging the membrane by small cracks or even the full destruction

of the sample. In order to reach temperatures close to 2000 K considering our specific membrane geometry, a constant bias of approximately 2 V has been applied between two electrodes pairs. Each pair consists of two neighboring electrodes that are switched in parallel. During biasing, an increase of the current can be observed, corresponding to the desorption of residues.

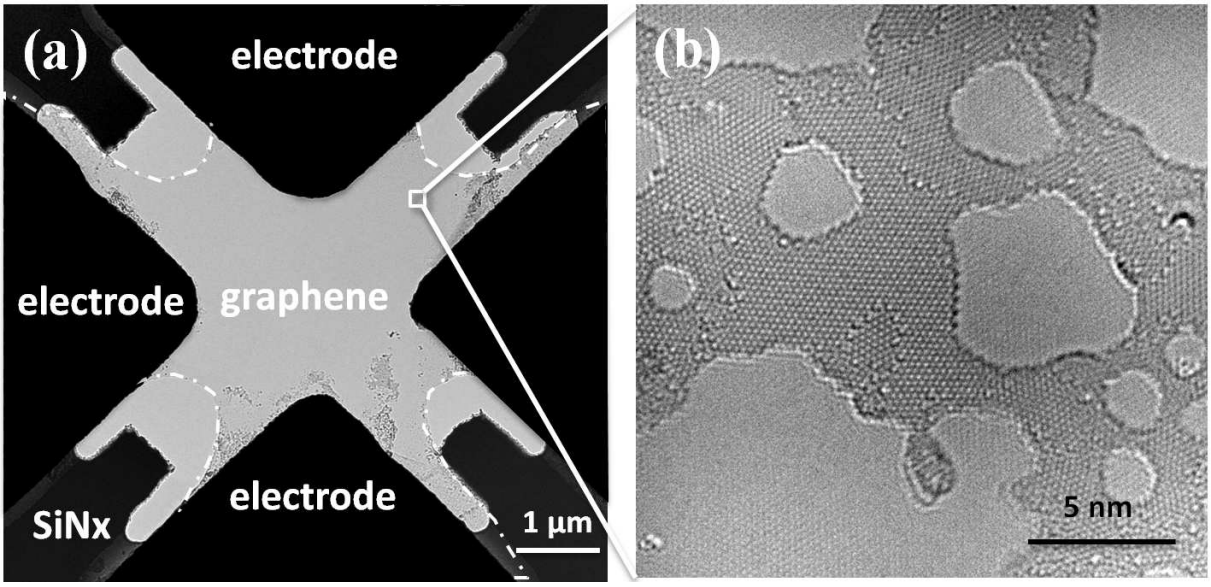

Fig. 4: (a) TEM overview image. The graphene membrane is indicated by the white broken line. It appears clean, apart from visible gray spots at the boundary. These small regions correspond to 3D carbon residues. (b) The HRTEM image reveals the presence of additional two-dimensional graphene patches. Again, they can be found only at the membrane's boundary. The underlying graphene lattice was removed applying a Fourier filter.

After a saturation of that behavior, the annealing has been considered to be finished and the membrane has been imaged for the first time (Fig. 4). Indeed, aside from few impurities at the boundary, the membrane appeared very clean. As also known from former experiments [13], the HR images reveal graphene patches formed on top of the graphene membrane. They are distributed on large areas along the membrane's entire boundary while the central membrane area appeared to be atomically clean. Interestingly, the in-situ transport measurements do not show a significant improvement on mobility compared to the previous experiment at gentle heating. At which extent the graphene patches may influence the transport measurement is not clarified yet. However, the formation of the graphene patches must originate from last residues that are rather present at the areas close to the gold electrodes. Due to increased heat dissipation, the temperature might be slightly lower there compared to the central region. We may speculate that the transformation of those potentially mobile hydrocarbons residues into fixed additional graphene layers occurs too fast for being able to drive them off. Obviously, obtaining the ideal temperature considering an appropriate annealing time is difficult. Furthermore, in contrast to single layer graphene, there is no experimental room temperature mobility value established in the literature for freestanding bilayer graphene. So it remains uncertain, which value should be expected after the successful application of Joule heating.

In order to investigate relative changes on the transport properties by implanted defects, the mobility does not necessarily need to be exceptionally high. For those investigations, we now consistently applied single layer graphene membranes. In order to avoid additional graphitic layers or damage by overheating, we do not exceed an annealing bias of 2.0 V. Furthermore, the annealing has to be interrupted after 30 min for practical limitations (limited microscope operation time). In order to avoid any redeposition of water molecules, we applied a constant background temperature of 175 °C by activating the integrated heating function of the specimen holder. This is important, because the high energetic beam electrons are able to crack potentially adsorbed water molecules into free radicals of hydrogen and oxygen. Those can easily initialize chemical etching processes accompanied with the systematic perforation of the graphene membrane. Finally, when we started the implantation of defects at 300 kV, we continually measured the mobility, the carrier density and the sheet resistance. Sometimes, our measurements showed considerable fluctuations. Normally, this could be correlated with the observation of forming holes or cracks. We also obtained similar fluctuations directly after increasing the dose rate, but without recognizing any visible change on the graphene membrane. Fig. 5a shows a HRTEM image of the graphene surface taken after 100 min of irradiation.

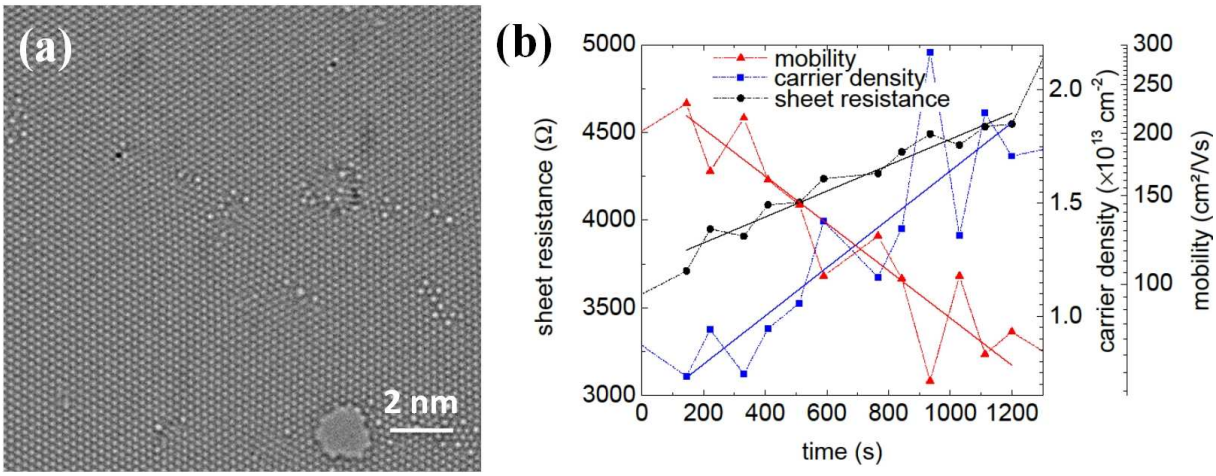

Fig. 5: (a) HRTEM image of the irradiated graphene membrane revealing a large number of defects. (b) Time-dependent behavior of the transport properties while irradiating constantly with $3.2 \cdot 10^8\, e\, \mu m^{-2} s^{-1}$ at 300 kV, with e being the electron charge.

Only time segments belonging to constant conditions, i.e., not during crack formations or changes on the dose rate, can be used for reasonably interpreting the measured transport properties. Such section is shown in Fig. 5b. As expected, during the defect implantation time, we find an exponential decay of the mobility and an increase of the sheet resistance. This suggests an increase of defect induced scattering processes. However, we also find an increase of the carrier density. As known from gate operated graphene devices [4], also the increasing number of carriers could be responsible for the decay in the mobility. The most probable origin of the increasing number of charge carriers might be the incorporation of impurity atoms into the defective sites [14].

4. Conclusions and Outlook

In summary, we presented an approach allowing the correlation between HRTEM imaging and the transport properties on a very basic level. At first, we discussed the realization of the most relevant technical issues, i.e., the magnetic field, the specimen holder and the sample carrier. Finally, we introduced one sample application demonstrating how directly visualized defective sites can be correlated to the electronic transport properties.

Further studies, i.e., density functional theory based simulations of the experimentally obtained defect distributions might help to clarify at which extent the decrease in mobility can be related purely to an increased lattice disorder and at which extend changes in the carrier density (most likely by doping on defective sites) has to be considered. The conversion from defective graphene into fully amorphized graphene is basically a matter of the electron dose and the irradiation time [15]. Our approach could help to clarify from the experimental perspective if such amorphized graphene specimens behave rather metallic or insulating [16–18].

Acknowledgment We thank Ilona Schwaiger, Susanne Menzel, Rudolf Rösch, Rainer Blood and Yakiv Men for their technical support. We thank our microscope operators Dr. Johannes Biskupek, Simon Kurasch and Dr. Dorin Geiger. A special thank goes to Prof. Dr. Jannik C. Meyer for his collaboration with respect to scientific questions and the microscope operation. Further we would like to thank our former students Tony Amende for realizing the specimen holder modifications and Johannes Wagner for realizing an optimized sample carrier design.

References

[1] A.K. Geim, "Graphene: status and prospects", *Science*, vol. 324, pp. 1530–1534, 2009.

[2] R.R. Nair, P. Blake, A.N. Grigorenko, K.S. Novoselov, T.J. Booth, T. Stauber, N.M.R. Peres, and A.K. Geim, "Fine structure constant defines visual transparency of graphene", *Science*, vol. 320, p. 1308, 2008.

[3] A.K. Geim and K.S. Novoselov, "The rise of graphene", *Nature Mater.*, vol. 6, pp. 183–191, 2007.

[4] K.I. Bolotin, K.J. Sikes, J. Hone, H.L. Stormer, and P. Kim, "Temperature-dependent transport in suspended graphene", *Phys. Rev. Lett.*, vol. 101, pp. 096802–1–4, 2008.

[5] F. Schedin, A.K. Geim, S.V. Morozov, E.W. Hill, P. Blake, M.I. Katsnelson, and K.S. Novoselov, "Detection of individual gas molecules adsorbed on graphene", *Nature Mater.*, vol. 6, pp. 652–655, 2007.

[6] S. Rumyantsev, G. Liu, M.S. Shur, R.A. Potyrailo, and A.A. Balandin, "Selective gas sensing with a single pristine graphene transistor", *Nano Lett.*, vol. 12, pp. 2294–2298, 2012.

[7] O. Leenaerts, B. Partoens, and F.M. Peeters, "Adsorption of H_2O, NH_3, CO, NO_2, and NO on graphene: a first-principles study", *Phys. Rev. B*, vol. 77, pp. 125416–1–6, 2008.

[8] S.T. Pantelides, Y. Puzyrev, L. Tsetseris, and B. Wang, "Defects and doping and their role in functionalizing graphene", *MRS Bulletin*, vol. 37, pp. 1187–1194, 2012.

[9] A. Zobelli, A. Gloter, C.P. Ewels, G. Seifert, and C. Colliex, "Electron knock-on cross section of carbon and boron nitride nanotubes", *Phys. Rev. B*, vol. 75, pp. 245402–1–9, 2007.

[10] L.J. Van der Pauw, "A method of measuring specific resistivity and Hall effect of discs of arbitrary shape", *Philips Res. Repts*, vol. 13, pp. 1–9, 1958.

[11] J.C. Meyer, C.O. Girit, M.F. Crommie, and A. Zettl, "Hydrocarbon lithography on graphene membranes", *Appl. Phys. Lett.*, vol. 92, pp. 123110–1–3, 2008.

[12] B. Westenfelder, J.C. Meyer, J. Biskupek, G. Algara-Siller, L.G. Lechner, J. Kusterer, U. Kaiser, C.E. Krill III, E. Kohn, and F. Scholz, "Graphene-based sample supports for in situ high-resolution TEM electrical investigations", *J. Phys. D: Appl. Phys.*, vol. 44, pp. 055502–1–7, 2011.

[13] B. Westenfelder, J.C. Meyer, J. Biskupek, S. Kurasch, F. Scholz, C.E. Krill, and U. Kaiser, "Transformations of carbon adsorbates on graphene substrates under extreme heat", *Nano Lett.*, vol. 11, pp. 5123–5127, 2011.

[14] H. Terrones, R. Lv, M. Terrones, and M.S. Dresselhaus, "The role of defects and doping in 2D graphene sheets and 1D nanoribbons", *Rep. Prog. Phys.*, vol. 75, pp. 062501–1–31, 2012.

[15] J. Kotakoski, A.V. Krasheninnikov, U. Kaiser, and J.C. Meyer, "From point defects in graphene to two-dimensional amorphous carbon", *Phys. Rev. Lett.*, vol. 106, pp. 105505–1–4, 2011.

[16] A. Kumar, M. Wilson, and M.F. Thorpe, "Amorphous graphene: a realization of Zachariasen's glass", *J. Phys.: Condens. Matter*, vol. 24, pp. 485003–1–7, 2012.

[17] E. Holmström, J. Fransson, O. Eriksson, R. Lizárraga, B. Sanyal, S. Bhandary, and M.I. Katsnelson, "Disorder-induced metallicity in amorphous graphene", *Phys. Rev. B*, vol. 84, pp. 205414–1–5, 2011.

[18] D. Van Tuan, A. Kumar, S. Roche, F. Ortmann, M.F. Thorpe, and P. Ordejon, "Insulating behavior of an amorphous graphene membrane", *Phys. Rev. B*, vol. 86, pp. 121408–1–5, 2012.